CHAPTER 4 BEVELED UWB MONOPOLE ANTENNA WITH SLOT LOADED SEMI-CIRCULAR LIKE GROUND PLANE

4.1 Introduction

This chapter presents an UWB monopole antenna configuration. It is designed to overcome the problems of antenna geometry complexities associated with fractal antenna structure discussed in previous chapter and for bandwidth enhancement.

The frequency domain and time domain analysis of the monopole antenna is carried out by using Ansoft HFSS [477] and CST Microwave Studio software [478] respectively. A brief description about the features of these simulation softwares is already presented in chapter three.

A planar beveled monopole antenna with slot loaded semicircular like ground plane is presented. The shape of the radiator is derived from a conventional rectangular monopole antenna by the application of beveling technique to its lower portions. The conventional partial rectangular ground plane is also replaced by a semi-circular like ground plane. This modified ground plane is loaded with a pair of rectangular slots. The combination of above mentioned three techniques resulted into achieving wider bandwidth.

4.2 Antenna Design

The geometry of the designed antenna is shown in Figure 4.1. The antenna is printed on a FR4 substrate having a relative permittivity of 4.4, loss tangent of 0.002 and thickness of 1.6mm. The size of the FR4 substrate used is $L_{sub} \times W_{sub}$. The designed antenna is derived from a conventional rectangular monopole antenna with partial rectangular ground plane. The dimensions of the rectangular patch are calculated by using the following standard antenna design equations [476]:

$$W = \frac{c}{2f_c\sqrt{\frac{\varepsilon_r+1}{2}}} \tag{49}$$

$$\varepsilon_{reff} = \frac{\varepsilon_r+1}{2} + \frac{\varepsilon_r+1}{2}\left[1+12\frac{h}{W}\right]^{-\frac{1}{2}} \tag{50}$$

$$L_{eff} = \frac{c}{4f_c\sqrt{\varepsilon_{reff}}} \tag{51}$$

$$\Delta L = 0.412h\frac{\left(\varepsilon_{reff}+0.3\right)\left(\frac{W}{h}+0.264\right)}{\left(\varepsilon_{reff}-0.258\right)\left(\frac{W}{h}+0.8\right)} \tag{52}$$

$$L = L_{eff} - 2\Delta L \tag{53}$$

Where, W = Width of radiating patch,

c = Speed of light,

f_c = Lower cutoff frequency,

ε_r = Relative dielectric constant of the substrate,

ε_{reff} = Effective dielectric constant,

h = height of substrate,

L_{eff} = Effective length of radiating patch,

ΔL = Delta length of radiating patch,

L = Actual length of radiating patch

The designed antenna structure comprises a dual edge tapered radiating patch, modified microstrip feedline and slot loaded semi-circular like ground plane. The dual edge tapered radiating patch consists of a rectangular patch and two trapezoidal patches. The antenna structure is fed by a 50 Ω microstrip line. The dimensions of the feed line are calculated using the standard feedline equations. The upper section of the feed line is tapered for impedance matching improvement. The optimized dimensions of the designed antenna are listed in Table 4.1.

The trapezoidal sections are generated by the application of beveling technique to the radiating edges of two lower subsections (Section II and III) generated after the division of rectangular patch antenna into three sections along its radiating edge. The beveling technique is applied for the smooth transitions between the feedline and radiating patch resulting into bandwidth enhancement.

During the evolution of the designed antenna structure, five intermediate or deriving configurations are achieved. The five intermediate stages are shown in Figure 4.2(a)-(e). In first stage, Antenna I, is the conventional rectangular patch antenna fed by a modified microstrip feedline and having partial rectangular ground plane. Before moving towards the second stage, the rectangular patch is divided into three sub sections i.e. section I, section II and section III along its radiating edges. Thereafter, the radiating edges of the section III are beveled or tapered for bandwidth enhancement due to smooth transitions of modes from the feedline to the radiating patch. After this, the radiating edges of section II are also beveled for improvement in impedance matching resulting into further bandwidth enhancement.

During the transition from third to fourth stage, the partial rectangular ground plane is replaced by a semi-circular like ground plane for the smooth transition of higher modes between the ground plane and radiating patch. At the final stage, the semicircular like ground plane is loaded with a pair of rectangular slots symmetrical to the feedline. These slots are etched to excite additional resonance a higher frequency. The length of these rectangular slots is calculated by using the following equation:

$$L_{slot} = \frac{c}{f_r \sqrt{\frac{\varepsilon_r + 1}{2}}} \tag{54}$$

where,

L_{slot} = length of the rectangular slot = 2×(slot_l+slot_w)
f_r = higher resonance frequency = 15.8 GHz

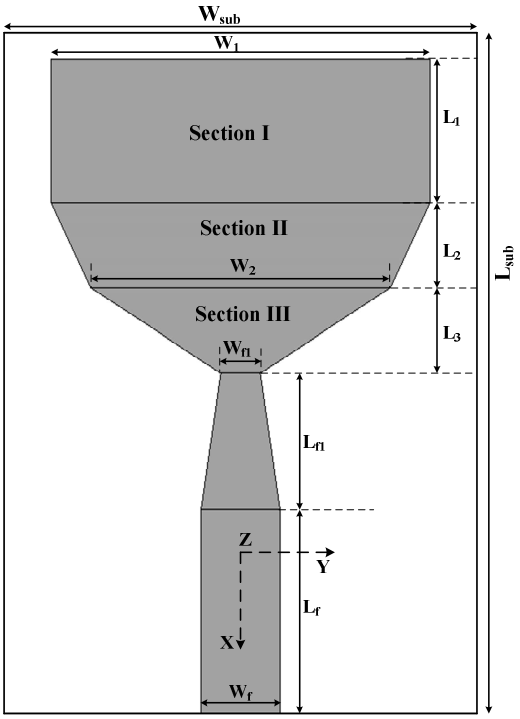

(a) Top View

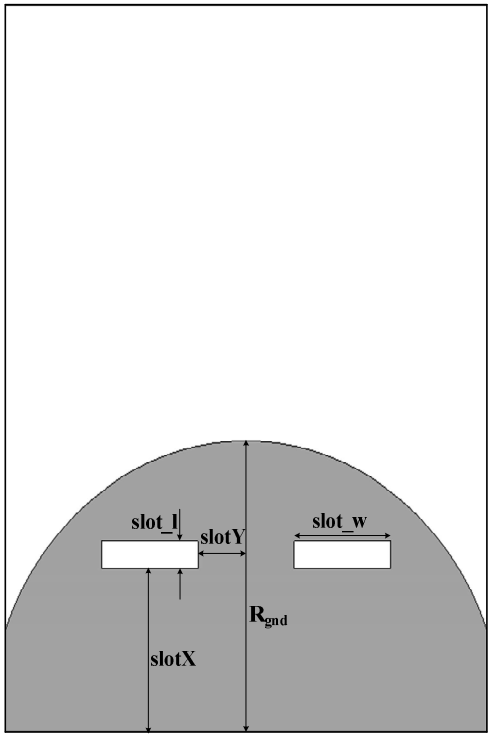

(b) Bottom View

Figure 4.1 Geometry of the beveled monopole antenna.

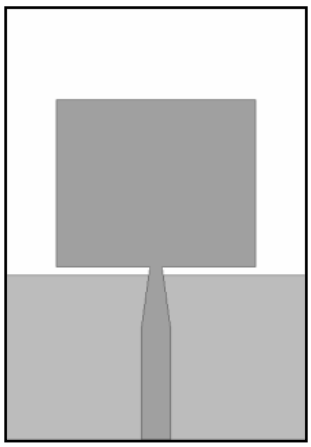

(a) Antenna I

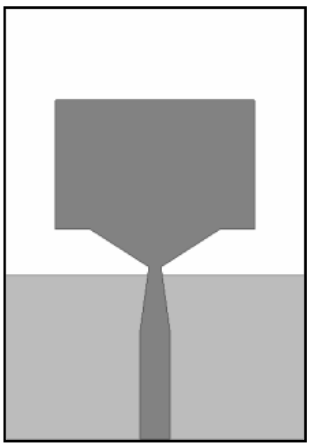

(b) Antenna II

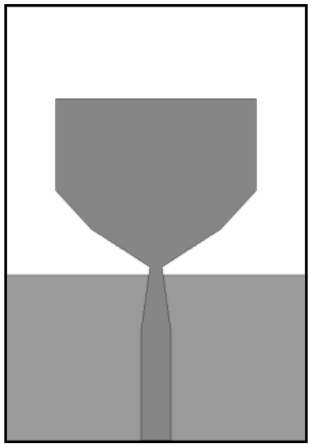

(c) Antenna III

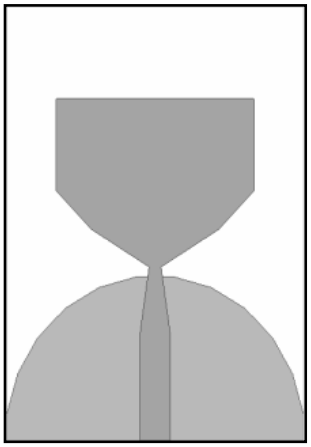

(d) Antenna IV

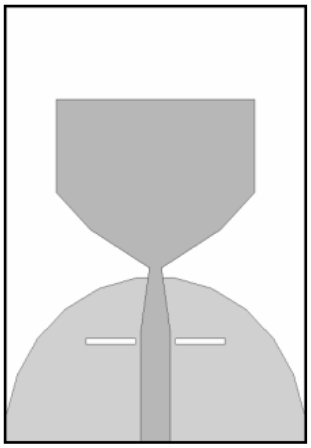

(e) Antenna V (designed antenna)

Figure 4.2 Deriving stages of beveled monopole antenna.

Table 4.1 Optimized dimensions of the beveled monopole antenna

Parameter	Dimension(mm)	Parameter	Dimension(mm)
L_{sub}	40	L_f	10
W_{sub}	30	L_{f1}	6
L_1	8.5	W_f	3
L_2	3.5	slot_l	0.5
L_3	3.5	slot_w	5
W_1	20	slotX	9
W_2	13	slotY	2
W_{f1}	1.2	R_{gnd}	15.2

4.3 Results and Discussion

This section discusses about the various results obtained during the analysis of the designed antenna structure. The results which are discussed in the following subsections include reflection coefficient characteristic, input impedance characteristic, radiation patterns, peak gain, efficiency and parametric analysis results in frequency domain. The time domain analysis subsection provides a description about the results like group delay, fidelity factor, isolation magnitude and phase to prove the suitability of the designed antenna for UWB applications.

4.3.1 Reflection Coefficient versus Frequency Characteristics

The comparison of the reflection coefficient versus frequency plots for five deriving stages of the designed antenna, shown in Figure 4.2, is demonstrated in Figure 4.3 and listed in Table 4.2. From Figure 4.3 and Table 4.2, it is observed that the conventional rectangular monopole antenna, Antenna I, has two operating bands i.e. 8.6334-16.3933 GHz and 17.6967-18.4483 GHz. In case of Antenna II, the first operating band of Antenna I got splitted into two operating bands i.e. 8.85-14.7324 GHz and 15.6112-16.5295 GHz with no significant effect on the second operating band of Antenna I. In addition to above mentioned two operating bands, an additional operating

band from 2.7476-5.8153 GHz is achieved. For Antenna III, two lower operating bands of Antenna II got merged into one operating band from 2.6745-14.332 GHz and the band from 17.6531-18.5742 GHz is shifted to 18.3383-19.0279 GHz without affecting the third operating band of antenna II. For Antenna IV, it is observed that the impedance bandwidth is enhanced significantly due to the shifting of edge frequencies of first operating band of antenna III from 2.6745 GHz to 2.436 GHz and 14.332 GHz to 14.6367 GHz. The second operating band of antenna III from 15.6583-16.7794 GHz is observed to get shifted towards higher frequency range from 16.3187-17.7843 GHz and the last operating band got disappeared for antenna IV. In case of antenna V, the slot loading of ground plane removed the second operating band of antenna IV and enhanced the impedance bandwidth of first operating band from 12.2007 GHz to 14.154 GHz by shifting the higher band edge towards higher frequency without affecting its lower band edge. Six resonances at the frequencies of 2.9, 7.1, 8.6, 11.6, 13.7 and 15.8 GHz are achieved in case of antenna V.

From Figure 4.3, it can be seen that the designed antenna structure has six resonances including three major resonances. Three major resonances at 2.9, 7.1 and 11.6 GHz are due to three sections of different dimensions. The first resonance of 2.9 GHz is achieved due to the overall size of the radiating patch. Second resonance at 7.1 GHz is achieved due to combined effect of the tapering of the middle and lowest section while the third resonance of 11.6 GHz is found due to the lowermost section of the radiating patch. The first two resonances are shifting towards the lower frequency due to the introduction of the modified ground plane with no effect on the higher resonance. The first resonance shifted towards lower frequency on loading the ground plane with rectangular slots.

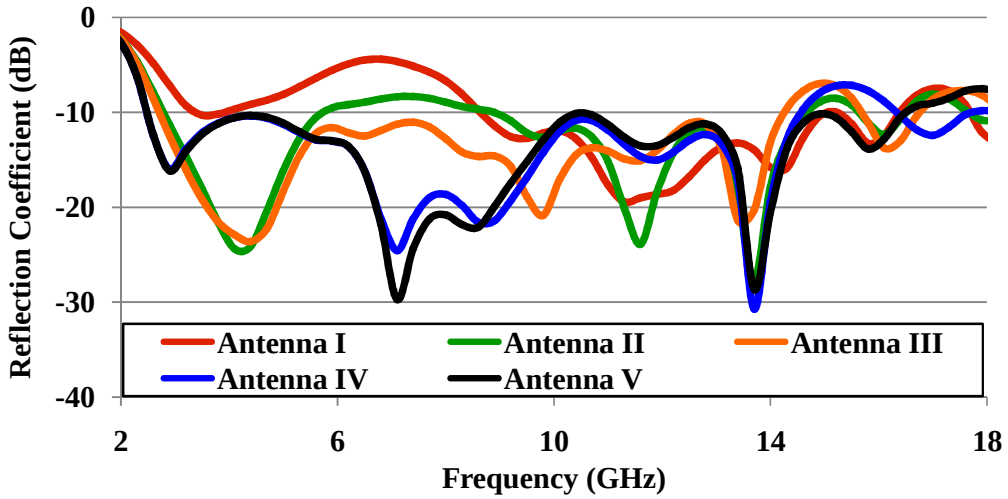

Figure 4.3 Comparison of reflection coefficient versus frequency plot for five deriving stages of the beveled monopole antenna structure

Table 4.2 Comparison of the bandwidth of five antenna configurations of beveled monopole antenna

Antenna	**I**	**II**	**III**	**IV**	**V**
f_{L1} (GHz)	8.63	2.75	2.67	2.44	2.45
f_{H1} (GHz)	16.39	5.82	14.33	14.64	16.6
BW_1 (GHz)	7.76	3.07	11.66	12.2	14.15
f_{L2} (GHz)	17.7	8.85	15.66	16.32	-
f_{H2} (GHz)	18.45	14.73	16.78	17.79	-
BW_2 (GHz)	0.75	5.88	1.12	1.47	-
f_{L3} (GHz)	-	15.61	18.34	-	-
f_{H3} (GHz)	-	16.53	19.03	-	-
BW_3 (GHz)	-	0.92	0.69	-	-
f_{L4} (GHz)	-	17.65	-	-	-
f_{H4} (GHz)	-	18.57	-	-	-
BW_4 (GHz)	-	0.92	-	-	-

Prior to the fabrication of the prototype of the designed beveled monopole antenna with slot loaded semi circular like ground plane, the HFSS simulation results are verified by using the FIT based CST MWS simulation tool. The prototype of the designed antenna structure is shown in Figure 4.4. The experimental measurement of the fabricated prototype is done by using Agilent E8364B PNA. The comparison

between the measured and simulated reflection coefficient characteristics is shown in Figure 4.5 and is also listed in Table 4.3. From Figure 4.5 and Table 4.3, it is observed that the experimental and simulation results are in good agreement. The discrepancy between the two simulation results is due to the different analytical techniques of simulation softwares [225]. The discrepancy among the simulated and experimental results can be attributed to the manufacturing tolerances, losses of SMA connector (SMA connector increases the return loss upto some extent) and scattering measurement environment.

4.3.2 VSWR versus Frequency Characteristic

The comparison among the simulated and experimental VSWR versus frequency characteristics for the designed antenna is depicted in Figure 4.6. It provides observations similar to those provided by reflection coefficient characteristics above.

(a) Top view (b) Bottom view

Figure 4.4 Prototype of the beveled monopole antenna.

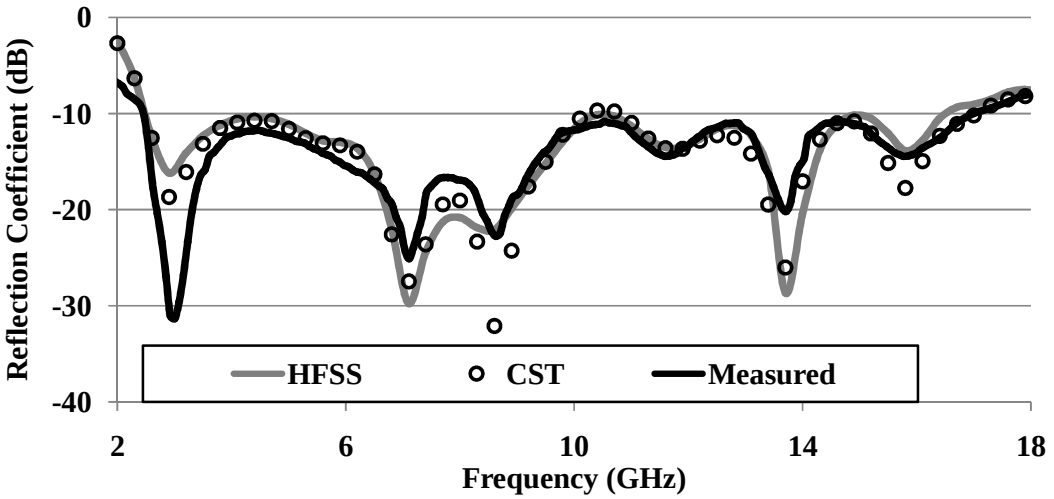

Figure 4.5 Comparison of simulated and measured reflection coefficient versus frequency characteristics for the beveled monopole antenna.

Table 4.3 Comparison of simulated and measured results for the beveled monopole antenna structure

S. No.	Method	Lower Cutoff, f_L (GHz)	Higher Cutoff, f_H (GHz)	Bandwidth	
				(GHz)	%
1.	HFSS	2.45	16.60	14.15	148.62
2.	CST	2.48	17.05	14.57	149.28
3.	Measured	2.4	17.1	14.7	150.77

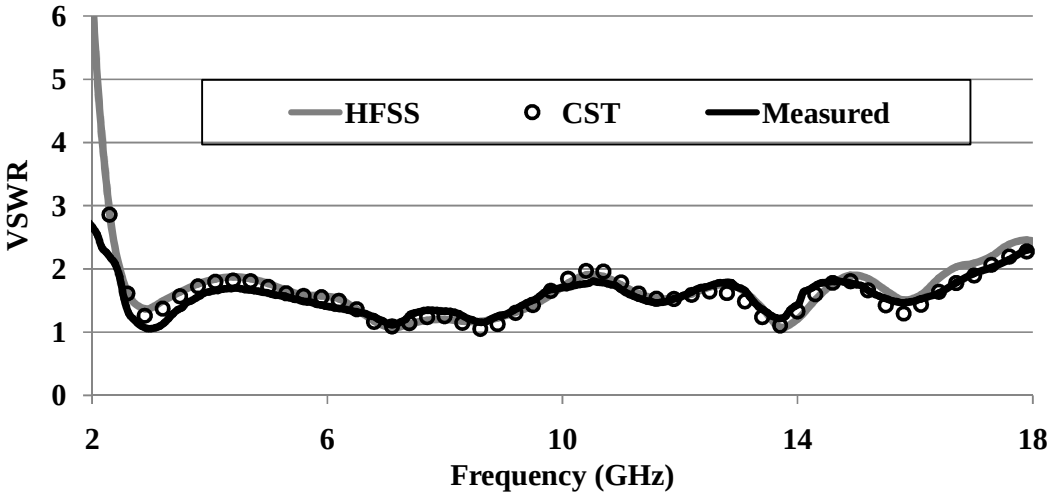

Figure 4.6 Comparison of simulated and measured VSWR versus frequency characteristics for the beveled monopole antenna.

4.3.3 Input Impedance versus Frequency Characteristic

The variation of real and imaginary parts of input impedance with frequency is shown in Figure 4.7. From Figure 4.7, it is observed that the real part of input impedance is varying around 50 Ω whereas the reactance is around 0 Ω in the whole operating frequency range. These variations of real and imaginary parts of input impedance are indicating that the designed antenna has an input impedance of approximately 50 Ω over the entire frequency range.

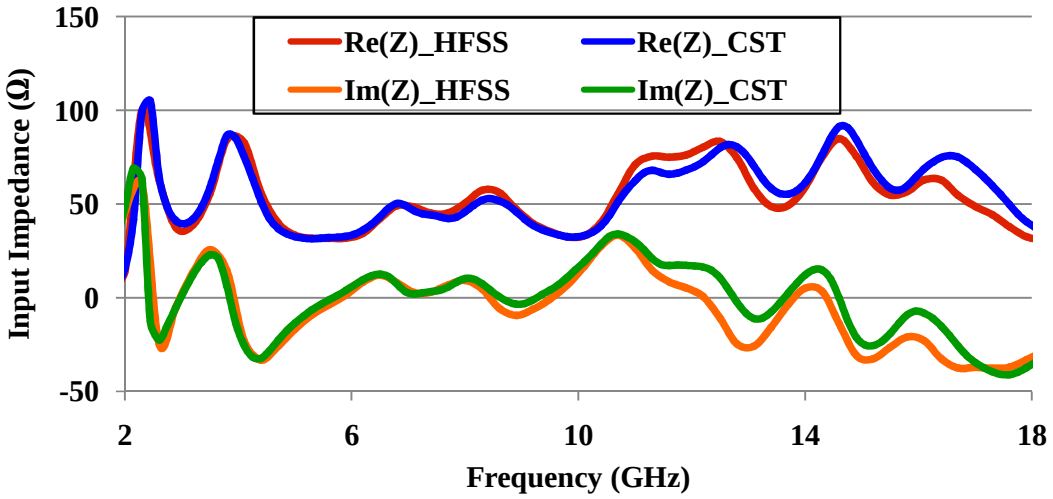

Figure 4.7 Simulated real and imaginary parts of the input impedance for the beveled monopole antenna.

4.3.4 Surface Current Density Distribution

The simulated surface current density plots of the designed antenna structure at its six resonance frequencies are shown in Figure 4.8. From Figure 4.8(a), it is observed that at the resonance of 2.9 GHz the surface current is distributed along the surface of the radiating patch, feedline and the ground plane. Less current density is observed at the upper non-radiating edge of the patch and the lower edges of the ground plane. At the resonance of 7.1 GHz, shown in Figure 4.8(b), the current density is observed to be

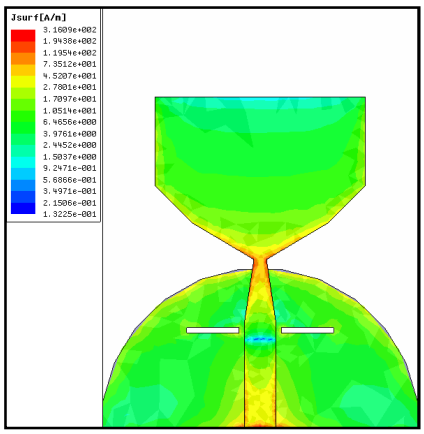

(a) 2.9 GHz

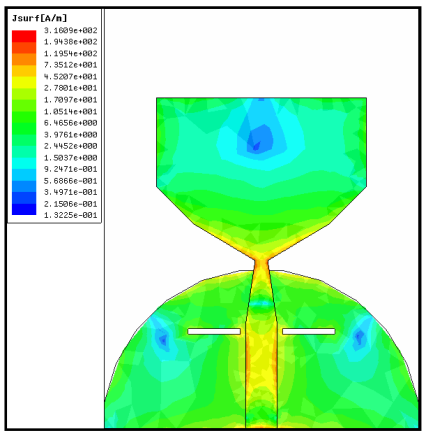

(b) 7.1 GHz

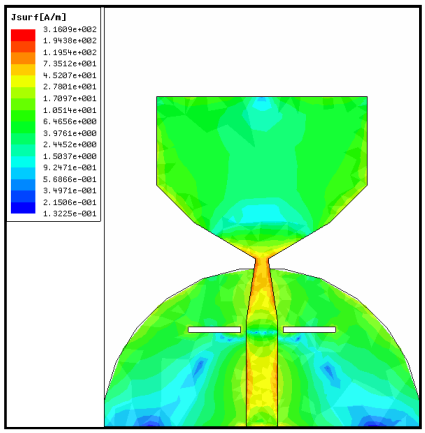

(c) 8.6 GHz

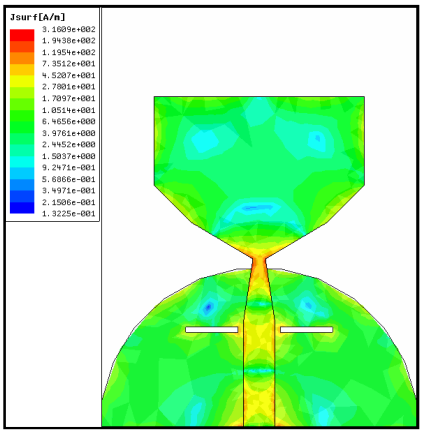

(d) 11.6 GHz

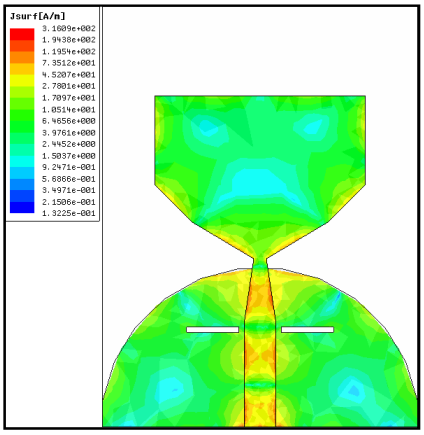

(e) 13.7 GHz

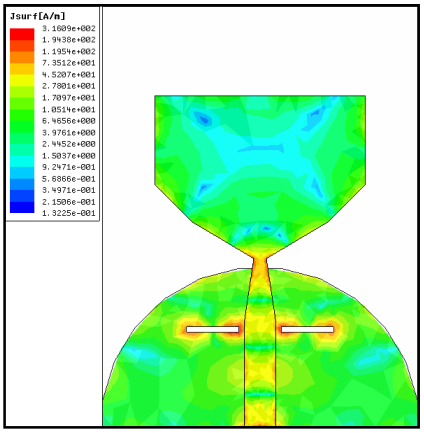

(f) 15.8 GHz

Figure 4.8 Simulated surface current distribution of the beveled monopole antenna structure at its six resonances.

concentrated along the two trapezoidal sections of radiating patch, feedline, above and below the slots in the ground plane. Null surface current density is observed inside the rectangular section of radiating patch, at the extreme right and left half of the ground plane.

In case of resonance at 8.6 GHz, shown in Figure 4.8(c), the current density is observed to be gathered along the radiating patch and upper half section of ground plane. Minimum surface current density is observed at the middle portion of the radiating patch and the extreme lower halves of the ground plane. Almost similar observations are made at the resonance of 11.6 GHz, shown in Figure 4.8(d). The area of null current density surface in the ground plane is reduced significantly. At the resonance of 13.7 GHz, shown in Figure 4.8(e), the surface current is observed to be zero in larger area inside the patch and ground plane as compared to that of 11.6 GHz.

For the last resonance at 15.8 GHz, illustrated in Figure 4.8(f), the current is mainly concentrated inside the feedline, ground plane and around the slots of the ground plane. The high density of current around slots is indicating that the resonance at 15.8 GHz is excited by these ground slots. Very less amount of current is present inside the radiating patch. The area of null current density surface is again reduced than the previously discussed resonance.

4.3.5 Far Field Radiation Patterns

The radiation pattern measurement setup for the designed antenna is shown in Figure 4.9. The antenna is placed along the x-axis in xy-plane. The E-plane pattern is measured in the direction of $\Phi=0^o$ and the H-plane pattern is measured along $\Phi=90^o$.

The measured radiation patterns of the designed antenna structure at its six resonance frequencies in both E-plane ($\Phi=0^o$) and H-plane ($\Phi=90^o$) are shown in Figure 4.10.

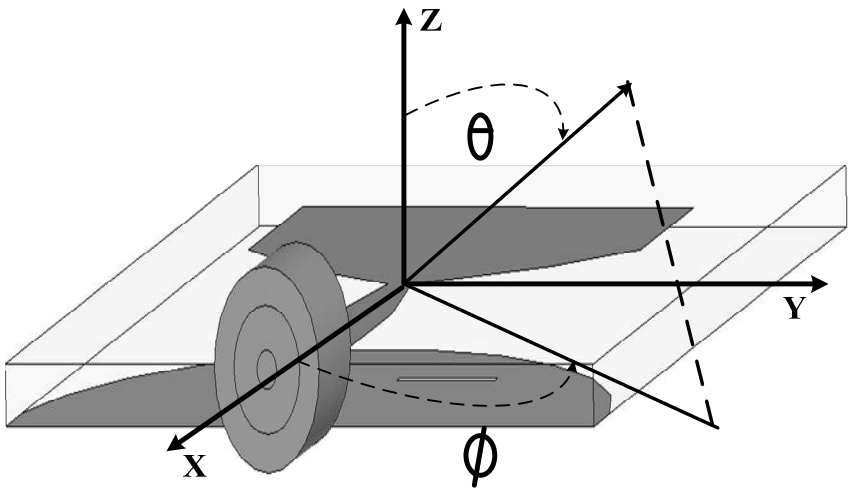

Figure 4.9 Radiation setup of the beveled monopole antenna

From Figure 4.10(a), it is observed that the designed antenna structure has omnidirectional radiation pattern in H-plane ($\Phi=90^{o}$) and dipole like pattern in E-plane ($\Phi=0^{o}$) at the resonance frequency of 2.9 GHz. In case of second resonance at 7.1 GHz, shown in Figure 4.10(b), the E-plane radiation pattern is observed to be distorted without any affect on the omnidirectional radiation pattern in H-plane.

At the third resonance of 8.6 GHz, shown in Figure 4.10(c), it is observed that the H-plane omnidirectional pattern is stable whereas the 8-shaped radiation pattern in E-plane is distorted.

In case of fourth resonance at 11.6 GHz, shown in Figure 4.10(d), the E-plane pattern is distorted significantly whereas the H-plane pattern is slightly distorted. The observations at the resonance of 13.7 GHz, shown in Figure 4.10(e), are similar to those at 11.6 GHz resonance.

At the last resonance of 15.8 GHz, shown in Figure 4.10(f), a quasi omnidirectional radiation patterns in both H-plane and E-plane are observed. The distortions in the radiation patterns at higher frequencies may be attributed to the excitation of higher modes at higher frequencies.

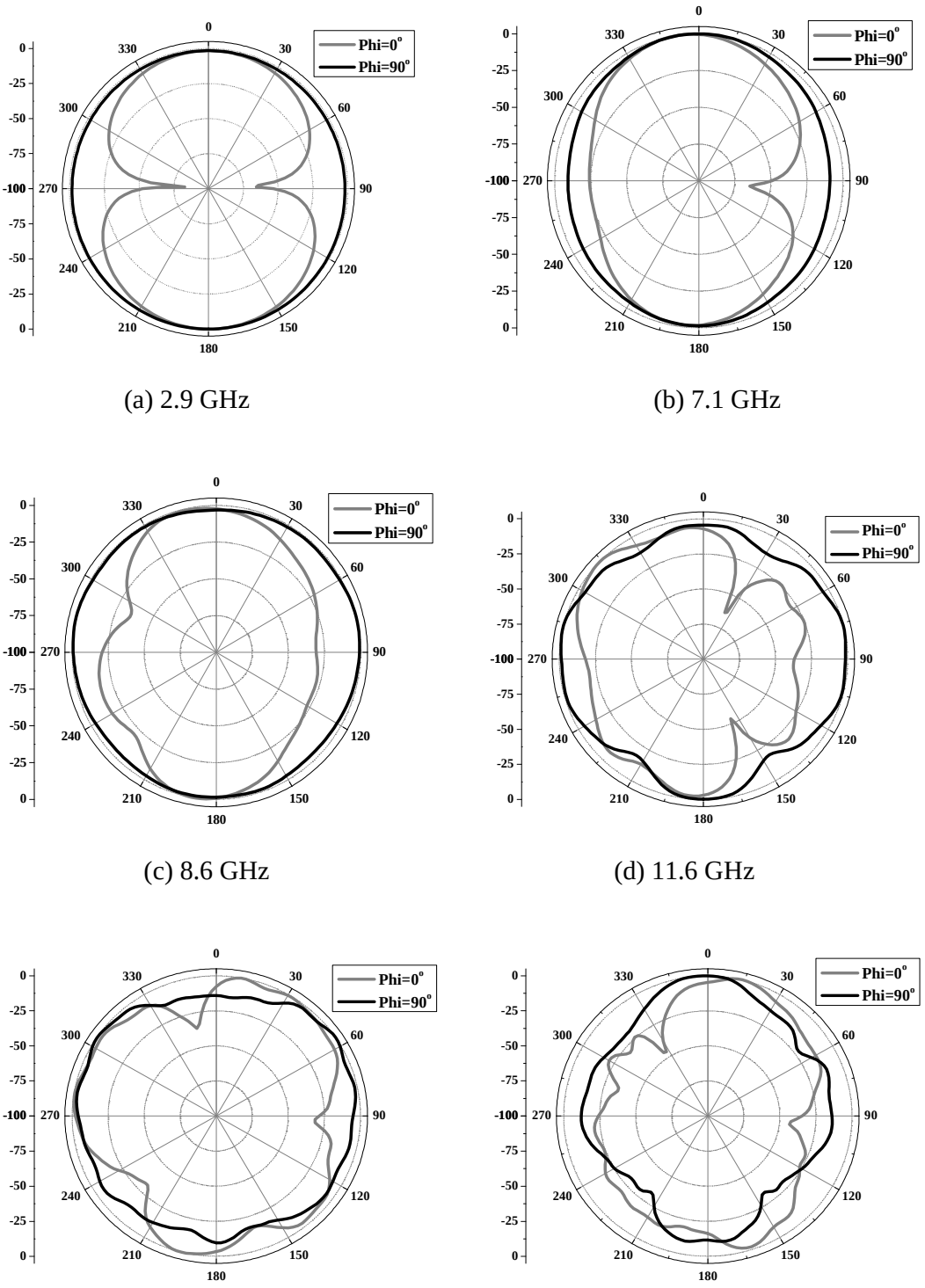

(a) 2.9 GHz

(b) 7.1 GHz

(c) 8.6 GHz

(d) 11.6 GHz

(e) 13.7 GHz

(f) 15.8 GHz

Figure 4.10 Measured radiation patterns of the beveled monopole antenna structure at its six resonances.

The measured co- and cross-polar radiation patterns in both E- and H-plane at all six resonance frequencies i.e. 2.9, 7.1, 8.6, 11.6, 13.7 and 15.8 GHz are shown in Figure 4.11. From Figure 4.11, it is observed that in E-plane at all resonances the cross-polar patterns are down by a minimum of 25 dB than the co-polar level. It is also observed that in H-plane the cross-polar level is less by 25 dB than the co-polar level for first two resonances whereas for remaining four resonances the level of cross-polar patterns is less than the level of co-polar pattern by a minimum of 0 dB and a maximum of 25 dB.

E-Plane H-Plane

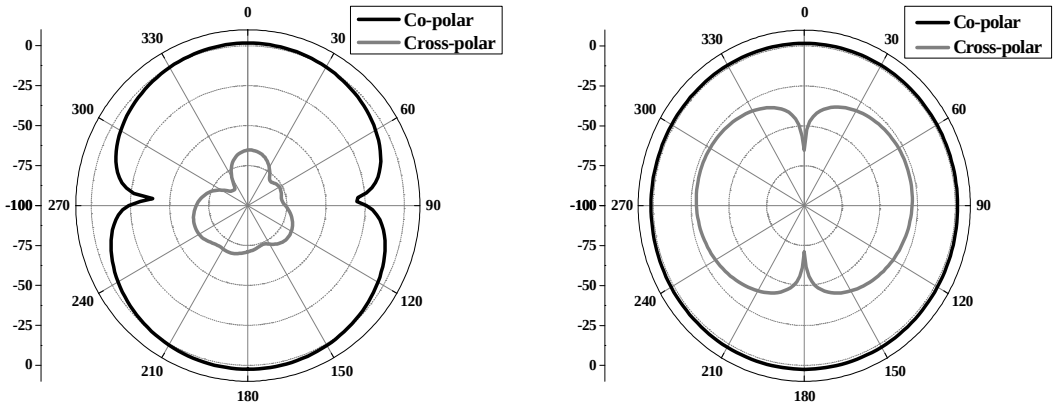

(a) 2.9 GHz

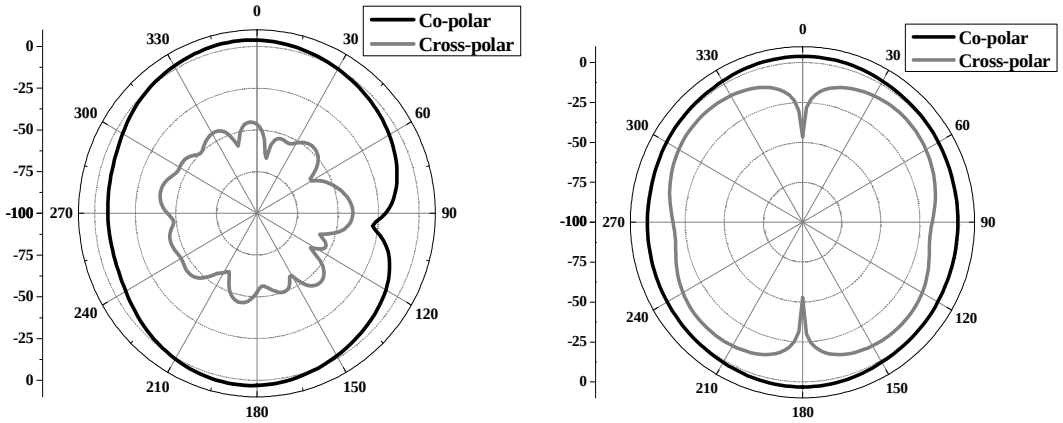

(b) 7.1 GHz

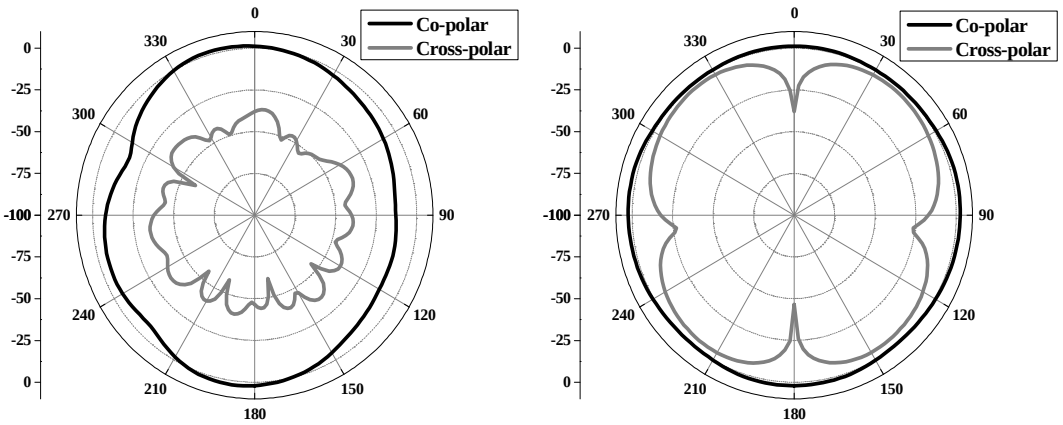

(c) 8.6 GHz

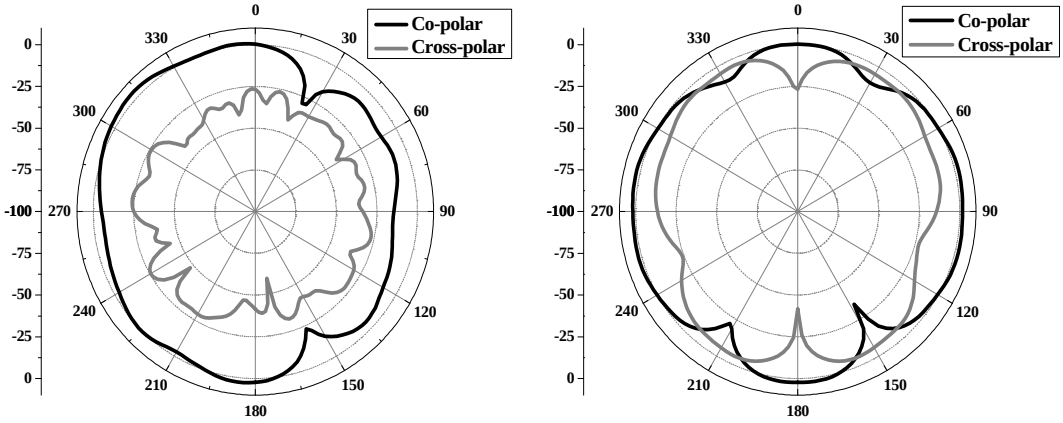

(d) 11.6 GHz

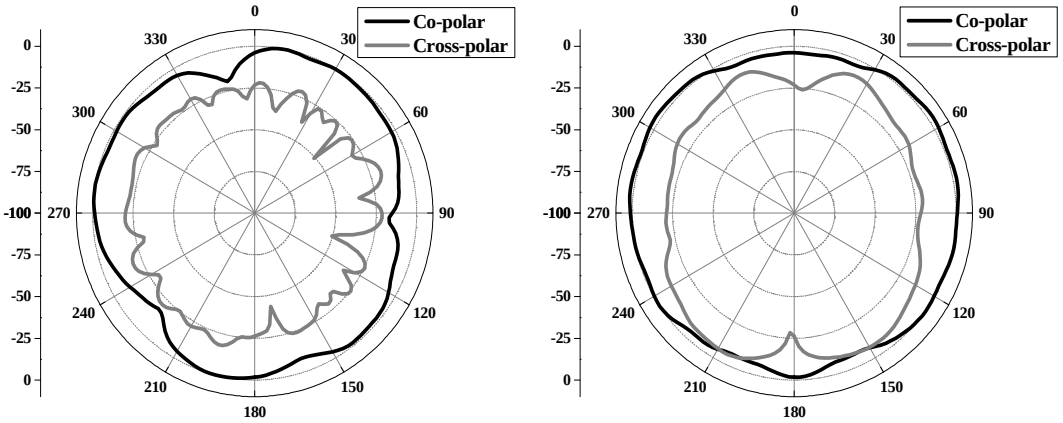

(e) 13.7 GHz

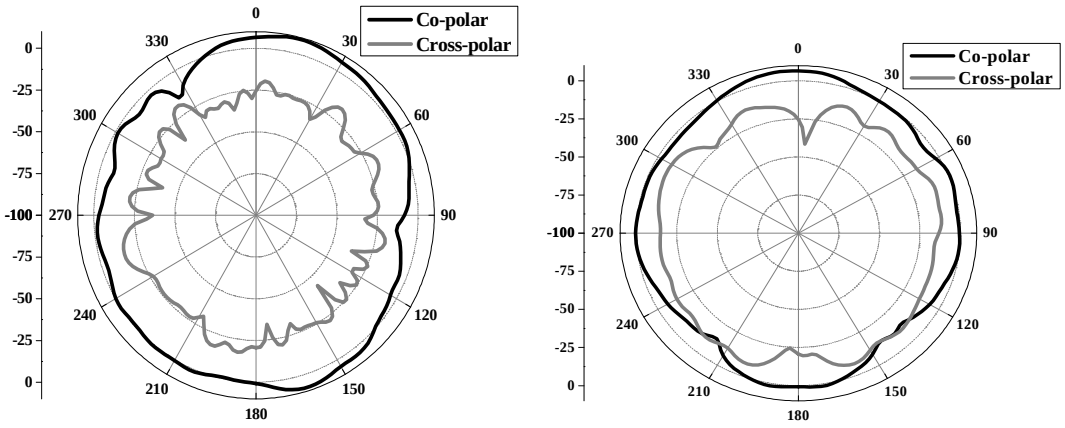

(f) 15.8 GHz

Figure 4.11 Measured co- and cross-polar radiation patterns of the beveled monopole antenna at its six resonance frequencies in both E- and H-plane.

4.3.6 Gain and Efficiency Characteristics

The variation of measured peak realized gain across the operating bandwidth is shown in Figure 4.12. From Figure 4.12, it is observed that the designed antenna has a maximum peak realized gain of 5.49 dB at 17 GHz and a minimum of 2.91 dB at 3.17 GHz with an average of 3.57 dB. The peak gain of the antenna is increasing with frequency due to the fact that at higher frequencies the patch dimensions are large in comparison to the wavelength.

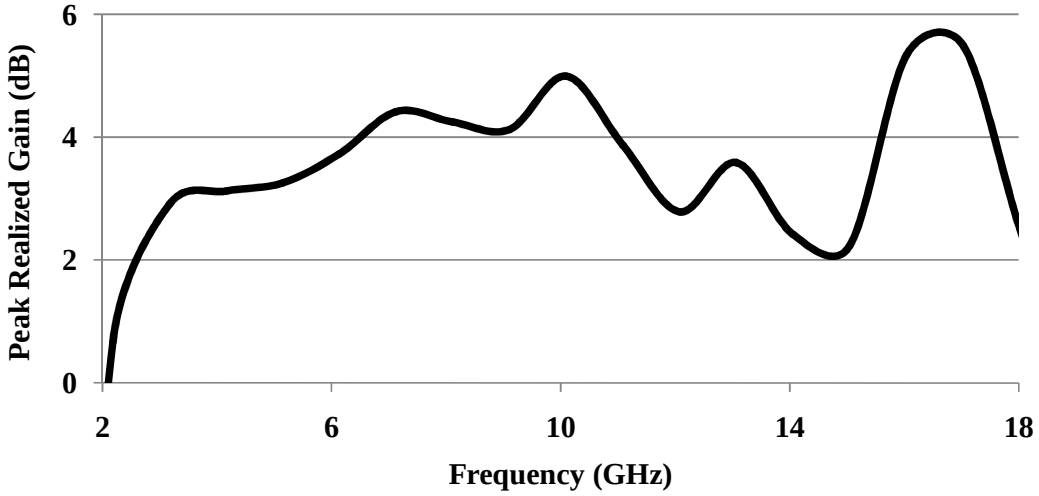

Figure 4.12 Measured peak realized gain of the beveled monopole antenna

The simulated total and radiation efficiencies of the designed antenna structure are shown in Figure 4.13. From Figure 4.13, it is observed that the designed antenna structure has a radiation efficiency of more than 75 % and a total efficiency of more than 70% in the entire frequency range. The efficiency of the designed antenna decreases as the frequency increases because of the varying performances of the radiating structures, substrate material and connectors at various frequencies.

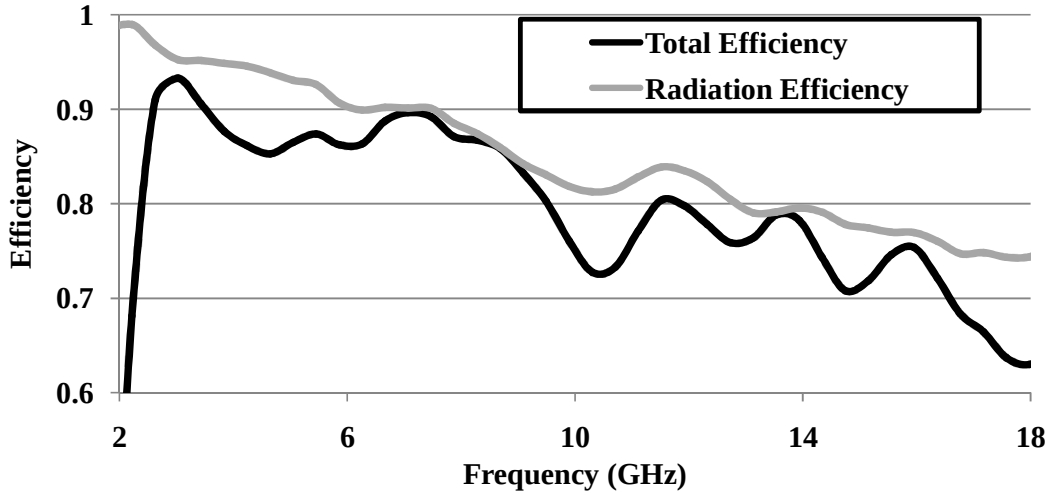

Figure 4.13 Simulated total and radiation efficiency of the beveled monopole antenna structure.

4.3.7 Time Domain Analysis

The time domain performance is an important characteristic of an UWB antenna. The time domain analysis is carried out by placing two identical designed antenna structures in two orientations i.e. face to face and side by side. The distance between two antenna structures in each configuration is fixed at 15 cm i.e. the farfield region of each antenna. The analysis is done by using CST MWS. One of those antenna structures is excited by a Gaussian pulse and the other antenna structure is used to receive the transmitted pulse. The normalized signal values of the excited and received pulses are shown in Figure 4.15. A well defined parameter fidelity factor is calculated by using

equation (46). From Table 4.4, it is observed that in face to face configuration the excited pulse is distorted significantly. In case of side by side configuration a good correlation between the excited and received pulse is observed which signifies low distortion.

(a) Face To Face

(b) Side By Side

Figure 4.14 Configurations of the beveled monopole for time domain analysis.

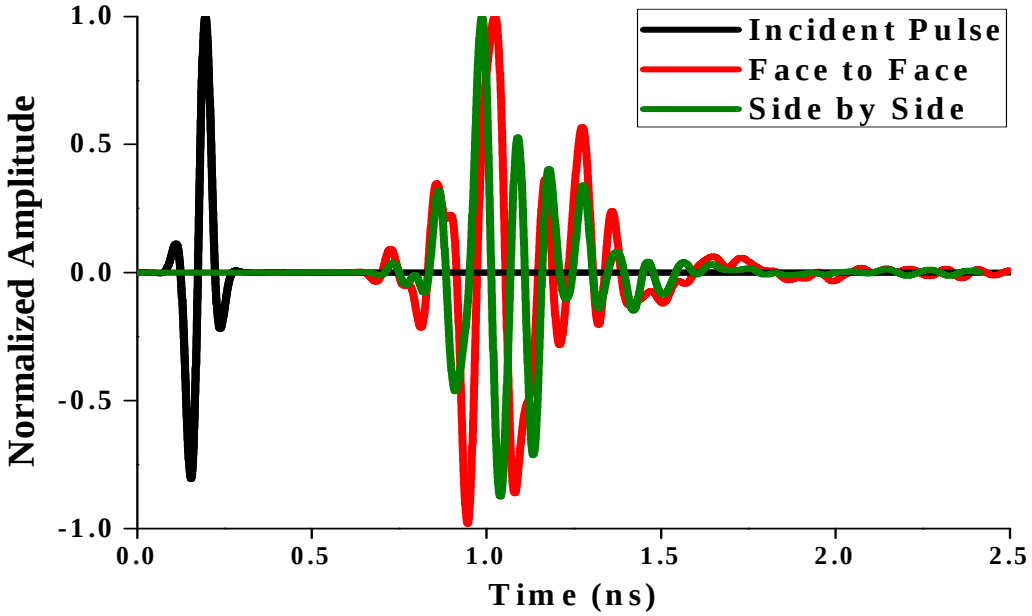

Figure 4.15 Time domain analysis of the beveled monopole antenna.

Table 4.4 Fidelity factor for two configurations of beveled monopole antenna

Configuration	Face to Face	Side by Side
Fidelity factor	54	75

The group delay is defined in previous chapter by equation (47). The simulated group delay for both orientations is shown in Figure 4.16. From Figure 4.16, it is observed that for both orientations the group delay is within the limits of 1 ns and is almost constant over the entire operating range.

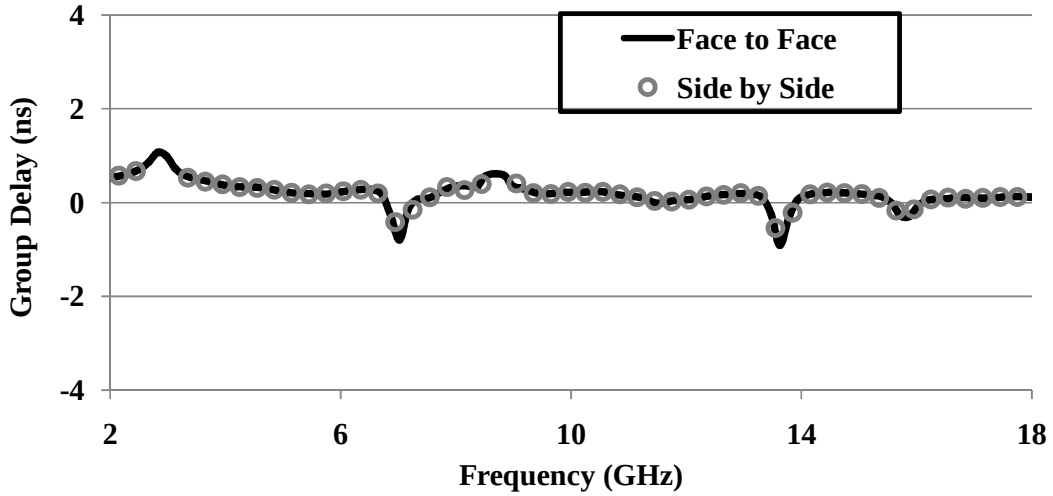

Figure 4.16 Simulated group delay of the beveled monopole antenna structure in two configurations.

The transfer function is also presented in above chapter by equation (48). The simulated amplitude of isolation, S_{21}, in both configurations is shown in Figure 4.17. From Figure 4.17, it is observed that the isolation for face to face configuration is varying between -20 dB and -50 dB. For side by side configuration, the isolation is lying between -20 dB and -40 dB.

The simulated phase of isolation, S_{21}, for each configuration of designed antenna structure is shown in Figure 4.18. It is observed that the phase is linear for both configurations which signifies the absence of 180^{o} phase shift in any configuration.

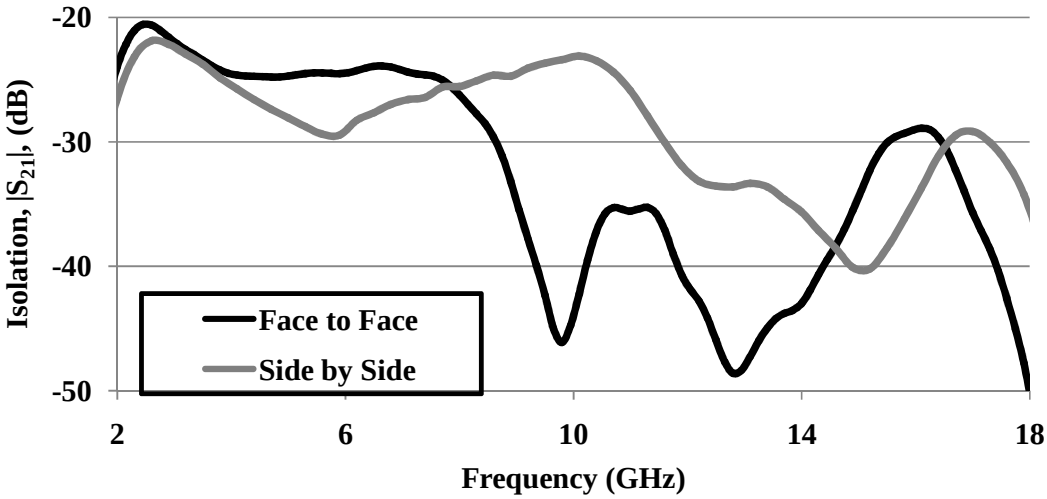

Figure 4.17 Simulated magnitude of isolation versus frequency plot for two configurations of the beveled monopole antenna

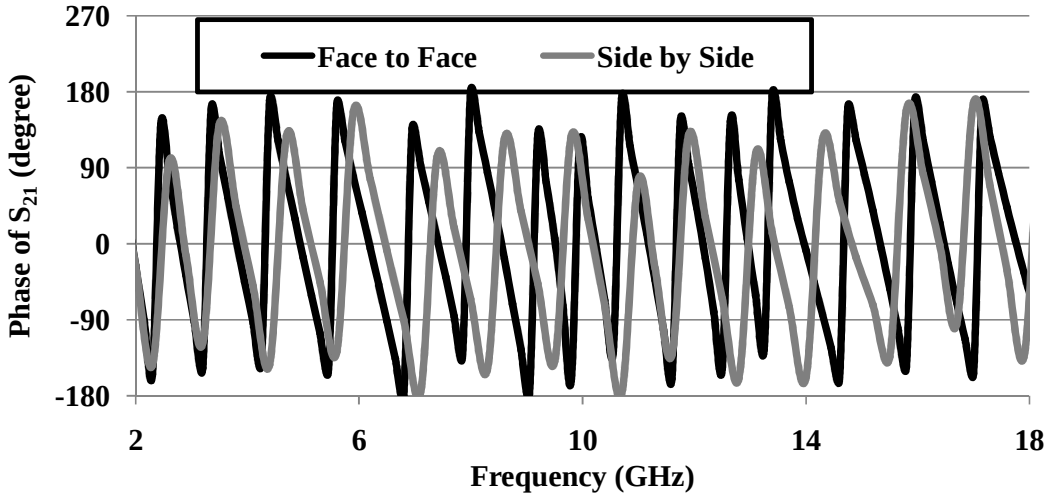

Figure 4.18 Simulated variation of phase of isolation with respect to frequency for two configurations of the beveled monopole antenna.

4.3.8 Effect of Different Substrates

During the parametric analysis of the designed antenna structure, three materials i.e. FR4 epoxy, Carbon Nano Tubes (CNT) [481] and $Ni_{0.2}Co_{0.2}Zn_{0.6}Fe_2O_4$ [482] are used as substrate. The comparison between the reflection coefficient versus frequency performance of the designed antenna structure for three substrate materials is depicted

in Figure 4.19. The comparison is also listed in Table 4.5. From Figure 4.19 and Table 4.5, it is observed that the impedance bandwidth of 15.87 (143.43 %) is achieved for CNT substrate having lowest value of relative permittivity and a bandwidth of 10.23 GHz (137.06 %) for $Ni_{0.2}Co_{0.2}Zn_{0.6}Fe_2O_4$ substrate having highest value of relative permittivity among three analyzed substrates. These transitions of the bandwidth (in case of CNT and $Ni_{0.2}Co_{0.2}Zn_{0.6}Fe_2O_4$) from that of FR-4 lead to a conclusion that the bandwidth is enhanced/reduced on using the substrate having lower/higher value of relative permittivity as stated by the standard microstrip antenna theory.

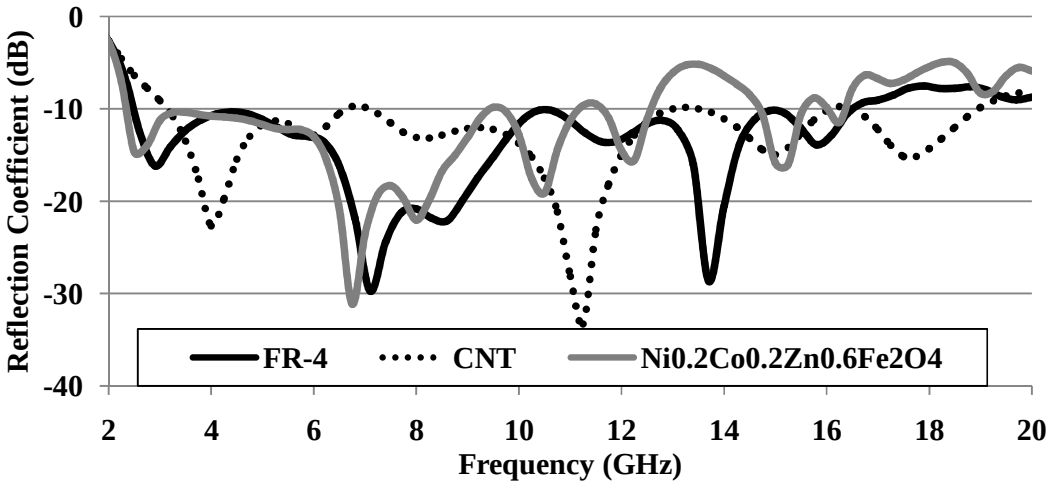

Figure 4.19 Comparison of reflection coefficient performance of the beveled monopole antenna with different substrate materials.

Table 4.5 Beveled monopole antenna performance for three different substrate materials

Substrate	**Carbon Nano Tubes**	**FR-4**	**$Ni_{0.2}Co_{0.2}Zn_{0.6}Fe_2O_4$**
ε_r	2.272	4.4	5.974
tan δ	0.0002	0.02	0.0023
f_L (GHz)	3.13	2.45	2.35
f_H (GHz)	19	16.6	12.58
BW (GHz)	15.87	14.15	10.23
% BW	143.43	148.62	137.04

4.3.9 Comparison with respect to previously reported structures

The designed antenna structure is compared with other antenna structures in terms of dimensions and the bandwidth, as shown in Table 4.6. It clearly indicates that the designed antenna structure is providing wider bandwidth performance with smaller dimensions in comparison to other structures. A typical size reduction of 58.19% and a fractional bandwidth of 150.77 % is achieved.

Table 4.6 Comparison between beveled monopole antenna and other monopole antenna structures

Antenna	**Bandwidth (GHz)**	**% BW**	**Size (mm^2)**	**% size reduction**
[228]	2.3-10.8	129.77	40×30	0
[258]	2.21-11.71	136.49	35×35	2.04
[252]	2.38-12.40	135.59	36×36	7.41
[62]	2.67-12	127.2	46×30	13.04
[264]	2.35-11.6	132.62	40×36	16.67
[225]	2.5-10.5	123.08	40×40	25
[56]	2.64-12	127.87	47×35.3	27.67
[108]	2.55-13.47	136.33	45×40	33.33
[240]	2.6-14.3	138.46	50×40	40
[86]	2.59-10.97	123.6	50×46	47.83
[275]	2.6-10.8	122.39	50×50	52
[55]	2.43-8.16	108.22	57.4×50	58.19
Designed Antenna	**2.4-17.1**	**150.77**	**40×30**	**-**

A compact microstrip-fed beveled monopole antenna is designed and analyzed. It is shown that by modifying the structure of radiating patch and ground plane, a wide bandwidth is achieved. The impedance bandwidth is further enhanced by etching two symmetrical rectangular slots with proper dimensions and position in the modified ground plane. The designed antenna has a simple configuration and easy fabrication process. The experimental results have proven that the realized antenna with a very compact size, simple structure, and wide bandwidth is a good candidate for UWB

applications. The designed antenna has nearly 12% more bandwidth and a typical size reduction upto 58% in comparison to the previously reported monopole antenna structures having approximately same lower band edge frequency. It will find its applications in radio determination applications, Railway applications(2.446-2.454 GHz), RFID (2.446-2.454 GHz), Wideband Data Transmission Systems(2.400-2.4835 GHz), satellite applications, Mobile applications, defence systems, radars, BBDR(4.940-4.990 GHz), Satellite Navigation systems, WAS/RLANS, RTTT (5.795-5.815 GHz), ITS(5.875-5.925 GHz. 5.855-5.875 GHz), Doppler Navigation aids, etc. [483]

The design of beveled UWB monopole antenna reduced the geometry complexities and enhanced the impedance bandwidth. To widen the impedance bandwidth further, a crescent dipole antenna is presented in the next chapter.